THE JOURNAL OF PHYSICAL CHEMISTRY LETTERS
A JOURNAL OF THE AMERICAN CHEMICAL SOCIETY

pubs.acs.org/JPCL Letter

Controlling the Dynamics of Three Electron Spin Qubits in a Donor–Acceptor–Radical Molecule Using Dielectric Environment Changes

Haochuan Mao, Ryan M. Young, Matthew D. Krzyaniak, and Michael R. Wasielewski*

Cite This: *J. Phys. Chem. Lett.* 2021, 12, 2213–2218 Read Online

ACCESS | Metrics & More | Article Recommendations | Supporting Information

ABSTRACT: Photogenerated entangled electron spin pairs provide a versatile source of molecular qubits. Here, we examine the spin-dependent dynamics of a covalent donor–acceptor–radical molecule, D-A-R$^{\bullet}$, where the donor chromophore (D) is *peri*-xanthenoxanthene (PXX), the acceptor (A) is pyromellitimide (PI), and the radical (R$^{\bullet}$) is α,γ-bisdiphenylene-β-phenylallyl (BDPA). Selective photoexcitation of D within D-A-R$^{\bullet}$ in butyronitrile/propionitrile at 140 K and butyronitrile at 105 K results in the spin-selective reactions D-A-R$^{\bullet}$ → D$^{\bullet+}$-^{1}(A$^{\bullet-}$-R$^{\bullet}$) and D$^{\bullet+}$-^{3}(A$^{\bullet-}$-R$^{\bullet}$). Subsequently, at 140 K, D$^{\bullet+}$-^{1}(A$^{\bullet-}$-R$^{\bullet}$) → D$^{\bullet+}$-A-R^{-}, whereas D$^{\bullet+}$-^{3}(A$^{\bullet-}$-R$^{\bullet}$) → D-A-R$^{\bullet}$. In contrast, at 105 K, D$^{\bullet+}$-^{3}(A$^{\bullet-}$-R$^{\bullet}$) → ^{3}*D-A-R$^{\bullet}$ and D-A-R$^{\bullet}$. Time-resolved EPR spectroscopy shows that ^{3}*D-A-R$^{\bullet}$ is highly spin-polarized, where the $m_s = \pm 1/2$ spin sublevels of the doublet–quartet manifolds are selectively populated. These results demonstrate dielectric environment control over different spin states in the same molecule.

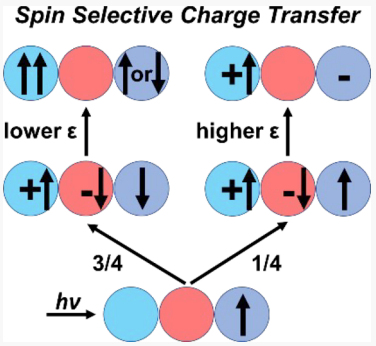

Quantum information science (QIS) is drawing increasing attention for its potential to provide new computation, communication, and sensing technologies.[1−3] Efforts are accelerating to identify and characterize new molecular systems to serve as qubits in these applications.[4,5] Taking advantage of synthetic tunability[6,7] and ease of spin-state readout by using microwave pulses,[8−10] electron spins in molecular systems have motivated chemists to achieve advances in extending coherence lifetimes[11−13] and scaling up the number of qubits.[14−17] These molecular systems employ multiple electron spin qubits comprising interacting organic radicals[8,9,18−21] and/or metal complexes[11,16,22−25] but are usually limited to thermally polarized electron spins[26] with well-defined initial spin states only available at high magnetic fields and temperatures <3 K.[18]

Subnanosecond photodriven electron transfer from a molecular donor to an acceptor has been shown to generate a radical pair having two entangled electron spins that can serve as a spin qubit pair (SQP) in a well-defined pure initial singlet quantum state,[27,28] even at room temperature.[29] Together with pulse electron paramagnetic resonance (pulse-EPR) techniques, we have shown that photogenerated SQPs can mediate quantum-state teleportation,[19] implement a CNOT gate,[20] and transfer polarization to a third spin.[30−33] Moreover, qubit-specific addressability can be achieved in an SQP system by using electronic *g*-factor engineering.[18,21,23]

While multiple potential QIS applications are possible by using such systems, different molecular designs are often required for each different application, which often entails complex chemical synthesis. However, since the SQP created by using a photoinduced charge transfer (CT) reaction is an ion pair, its energy is sensitive to the surrounding dielectric environment. Electron transfer theory predicts that changing the ion pair energy changes its formation and recombination rates.[34−36] Thus, the kinetic competition between SQP recombination and subsequent CT from the SQP to another molecule can be controlled by changing the dielectric environment of the medium surrounding the SQP.

In this work, we demonstrate different spin-dependent CT dynamics in a covalent electron donor–acceptor–radical molecular triad (D-A-R$^{\bullet}$, **1**, Scheme 1) by tuning the dielectric environment, where the donor chromophore (D) is *peri*-xanthenoxanthene (PXX), the acceptor (A) is pyromellitimide (PI), and the radical (R$^{\bullet}$) is α,γ-bisdiphenylene-β-phenylallyl (BDPA). PXX, PI, and BDPA were chosen because their redox potentials provide sufficient free energy of reaction[36] to carry out parallel spin-dependent charge transfer processes.

Following selective photoexcitation of D within D-A-R$^{\bullet}$ in butyronitrile/propionitrile (PrCN/EtCN) at 140 K and PrCN at 105 K, the spin-selective CT reactions D-A-R$^{\bullet}$ → D$^{\bullet+}$-^{1}(A$^{\bullet-}$-R$^{\bullet}$) and D$^{\bullet+}$-^{3}(A$^{\bullet-}$-R$^{\bullet}$) occur. These solvents and temperatures were chosen because D-A-R$^{\bullet}$ is soluble in these media and both solvents form optically clear glasses at the indicated temperatures. Subsequently, at 140 K, D$^{\bullet+}$-^{1}(A$^{\bullet-}$-R$^{\bullet}$) → D$^{\bullet+}$-A-R^{-}, whereas D$^{\bullet+}$-^{3}(A$^{\bullet-}$-R$^{\bullet}$) → D-A-R$^{\bullet}$. Importantly, we have shown previously that the spin dynamics of D$^{\bullet+}$-A-R^{-}

Received: January 8, 2021
Accepted: February 17, 2021
Published: February 25, 2021

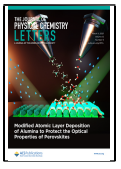

https://dx.doi.org/10.1021/acs.jpclett.1c00077
J. Phys. Chem. Lett. 2021, 12, 2213–2218

Scheme 1. Structures of 1H and 1

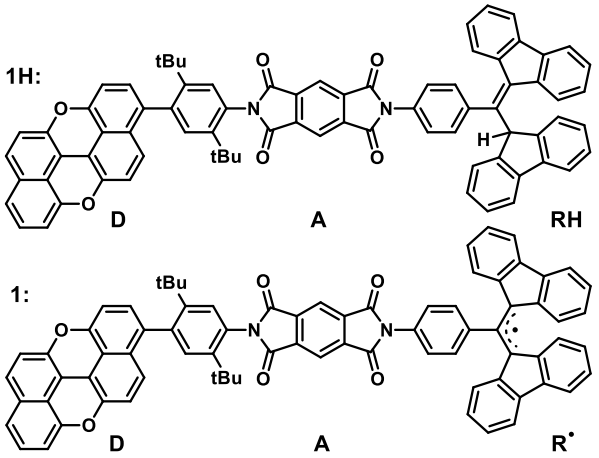

formation can be used to teleport a spin state initially prepared on R• to D•+.[19,37] In contrast, lowering the temperature to 105 K in PrCN results in the reaction D•+-^{3}(A•−-R•) → ^{3}*D-A-R• and D-A-R•, where the spin dynamics of the weakly coupled triplet−doublet pair ^{3}*D-A-R• strongly spin-polarizes R•, which we observe by time-resolved EPR (TREPR) techniques.[38,39] Thus, the latter reaction provides a means to initialize an electron spin qubit in a specific quantum state at modest temperatures. These results show that changing the dielectric environment of radical ion pair-based spin qubits can result in several outcomes useful to quantum information applications.

D-A-R• (**1**, Scheme 1) was prepared by quantitative oxidation of **1H**, which was synthesized by imide condensation of a BDPAH-PI monoanhydride onto a PXX functionalized with 2,5-di-*tert*-butylaniline (see the Supporting Information for details). Steady-state absorption spectra of **1** and **1H** are presented in Figure S1. The femtosecond transient absorption (fsTA) and nanosecond transient absorption (nsTA) spectrometers have been described previously.[40] Details of sample preparation and temperature control are summarized in the Supporting Information. The spin-dependent charge transfer pathways for each temperature are depicted in Figure 1. The specific radical ion pair energies were estimated by using the Weller equation[36] (see the Supporting Information) and will be discussed in the context of the transient spectroscopic data presented below.

Selective photoexcitation of D in **1** at 414 nm in 9/2 v/v PrCN/EtCN at 140 K immediately produces the excited state of the donor (^{1}*D), which is characterized by absorptions at 633 and 1140 nm, and stimulated emission at 482 and 518 nm (Figure 2a). The subsequent charge separation (CS) reaction ^{1}*D-A-R• → D•+-A•−-R• results in the appearance of an absorption at 723 nm resulting from the reduced acceptor (A•−)[41] and absorptions at 530 and 920 nm resulting from the oxidized donor (D•+).[42] Global fitting of the fsTA data using the spin-selective model in Figure 1a (see the Supporting Information) yields the species-associated spectra along with the rate constants (Figure S3). The rate constants for **1** at 140 K are summarized in Table 1. The CS reaction occurs with an observed rate constant $k_{CS1} = {}^1/_4k^S_{CS1} + {}^3/_4k^T_{CS1} = (56.3 \pm 0.8\ \text{ps})^{-1}$, which indicates the reaction yield is nearly quantitative given that the intrinsic lifetime of ^{1}*D is 4.5 ns.[43]

D•+-A•− is produced in an entangled singlet spin state due to strong exchange coupling between its two unpaired electron spins (see below). However, the spin configuration of A•− relative to R• is purely statistical, resulting in populations of 25% D•+-^{1}(A•−-R•) and 75% D•+-^{3}(A•−-R•). Thus, only the singlet secondary CS reaction, D•+-^{1}(A•−-R•) → D•+-A-R−, is spin-allowed[44] and is indicated by the appearance of the absorption of R− at 600 nm[44] with an observed rate constant $k^S_{CS2} + k^S_{CR1} = (17 \pm 2\ \text{ps})^{-1}$. D•+-A-R− then decays back to D-A-R• with an observed charge recombination (CR) rate constant $k^S_{CR2} = (690 \pm 10\ \text{ns})^{-1}$ (Figure S3). The CT rate constants for reference compound D•+-A•−-RH, **1H**, which lacks R• are not spin selective as defined for **1**; thus, $k_{CS1} = (49.5 \pm 0.5\ \text{ps})^{-1}$ and $k_{CR1} = (464 \pm 4\ \text{ps})^{-1}$ (Figure S5). For **1**, this implies that $k^S_{CS2} \gg k^S_{CR1}$, and thus $k^S_{CS2} + k^S_{CR1} \simeq k^S_{CS2}$.

Meanwhile, the 75% subpopulation, D•+-^{3}(A•−-R•), decays with an observed rate constant $k^T_{CR1} + k^T_{CR2} = (513 \pm 5\ \text{ps})^{-1}$.

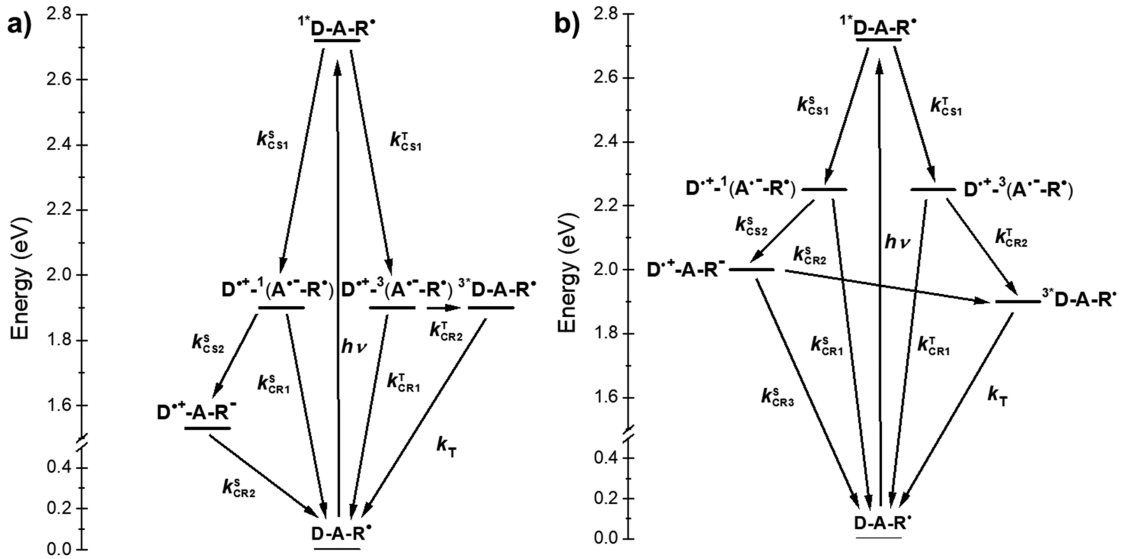

Figure 1. Kinetic pathways and energies for the relevant states of **1** in (a) 9/2 v/v PrCN/EtCN at 140 K assuming $\varepsilon_s = 3.4$ and in (b) PrCN at 105 K assuming $\varepsilon_s = 2.3$.

https://dx.doi.org/10.1021/acs.jpclett.1c00077
J. Phys. Chem. Lett. 2021, 12, 2213−2218

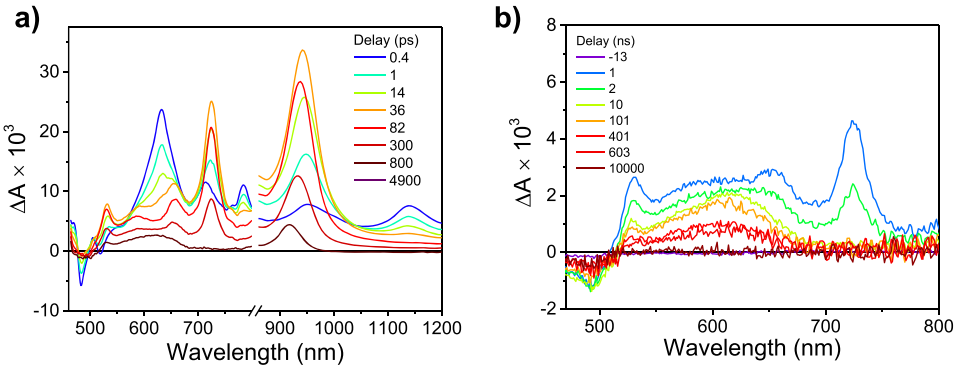

Figure 2. FsTA (a) and nsTA (b) transient absorption spectra of **1** in 9/2 PrCN/EtCN at 140 K following λ_{ex} = 450 nm excitation.

Table 1. Rate Constants

	1			**1H**	
rate constant	PrCN/EtCN 140 K	PrCN 105 K	rate constant	PrCN/EtCN 140 K	PrCN 105 K
k_{CS1}	$(56.3 \pm 0.8\ ps)^{-1}$	$(34.8 \pm 0.5\ ps)^{-1}$	k_{CS1}	$(49.5 \pm 0.5\ ps)^{-1}$	$(48.9 \pm 0.2\ ps)^{-1}$
k^S_{CS2}	$(17 \pm 2\ ps)^{-1}$	$(15 \pm 1\ ps)^{-1}$		–	–
k^S_{CR2}	$(690 \pm 10\ ns)^{-1}$	$(11.7 \pm 0.4\ ns)^{-1}$	k_{CR1}	$(464 \pm 4\ ps)^{-1}$	$(38.7 \pm 0.5\ ns)^{-1}$ (60%) $(228 \pm 4\ ns)^{-1}$ (40%)
k^T_{CR1}	$(513 \pm 5\ ps)^{-1}$			–	–
k^T_{CR2}	–	$(902 \pm 22\ ps)^{-1}$		–	–

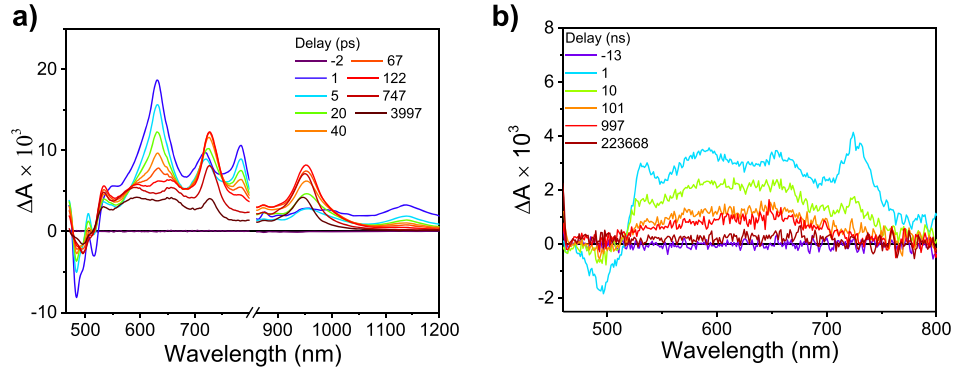

Figure 3. FsTA (a) and nsTA (b) transient absorption spectra of **1** in a PrCN glass at 105 K following λ_{ex} = 450 nm excitation.

Because the nsTA spectra (Figure 2b) show no measurable formation of ^{3}*D-A-R$^\bullet$, $k^T_{CR1} + k^T_{CR2} \simeq k^T_{CR1}$. Comparing k_{CR1} for **1H** with k^T_{CR1} for **1** shows that they are similar, thus implying that $k^S_{CR1} \simeq k^T_{CR1}$. Because D$^{\bullet+}$-^{3}(A$^{\bullet-}$-R$^\bullet$) → ^{3}*D-A-R$^\bullet$ does not compete kinetically with D$^{\bullet+}$-^{3}(A$^{\bullet-}$-R$^\bullet$) → D-A-R$^\bullet$, the energies of D$^{\bullet+}$-^{1}(A$^{\bullet-}$-R$^\bullet$) and D$^{\bullet+}$-^{3}(A$^{\bullet-}$-R$^\bullet$) at 140 K are most likely less than or equal to that of ^{3}*D-A-R$^\bullet$. The calculated energies of the radical ion pairs illustrated in Figure 1a show that this occurs when the solvent dielectric constant is $\varepsilon_s \geq 3.4$.

Lowering the temperature of **1** in PrCN to 105 K results in fsTA spectra (Figure 3a), whose global analysis yields the initial observed CS rate constant $k_{CS1} = (34.8 \pm 0.5\ ps)^{-1}$. The 25% subpopulation, D$^{\bullet+}$-^{1}(A$^{\bullet-}$-R$^\bullet$), charge separates further with a rate constant $k^S_{CS2} = (15 \pm 1\ ps)^{-1}$ to yield D$^{\bullet+}$-A-R$^-$, which decays with an observed CR rate constant $k^S_{CR2} + k^S_{CR3} = (11.7 \pm 0.4\ ns)^{-1}$ (Figure S4). The rate constant is much larger than that observed at 140 K. Lowering the temperature raises the energies of the radical ion pairs. Given that CR directly to the D-A-R$^\bullet$ ground state is far into the Marcus inverted region[34,35] of the rate vs free energy profile, the larger energy gap for CR to ground state at 105 K should result in k^S_{CR3} for **1** being smaller at 105 K relative to k^S_{CR2} at 140 K. The energy of D$^{\bullet+}$-^{1}(A$^{\bullet-}$-R$^\bullet$) is above ^{3}*D-A-R$^\bullet$ at 105 K, thus CR proceeds predominantly to ^{3}*D-A-R$^\bullet$ with $k^S_{CR2} + k^S_{CR3} \simeq k^S_{CR2}$ because CR to ^{3}*D-A-R$^\bullet$ is in the Marcus normal region. These assertions are based on the fact that the total reorganization energy, λ, for D$^{\bullet+}$-A-R$^-$ → D-A-R$^\bullet$ is ∼0.4 eV, given that typical internal reorganization energies for charge transfer reactions involving polycyclic aromatic molecules are ∼0.2 eV, while the solvent reorganization energy is negligible in very low dielectric constant media.[45] Note that D$^{\bullet+}$-A-R$^-$ is a doublet state with no spin polarization apart from that determined by the Boltzmann population of the spin states of D$^{\bullet+}$; thus, it does not contribute to the spin dynamics observed by TREPR at 105 K (see below). The rate constants for **1** at 105 K are summarized in Table 1.

At 105 K, the 75% subpopulation, D$^{\bullet+}$-^{3}(A$^{\bullet-}$-R$^\bullet$), charge recombines to both ^{3}*D-A-R$^\bullet$ and the ground-state D-A-R$^\bullet$ with the observed rate constant $k^T_{CR1} + k^T_{CR2} = (902 \pm 22\ ps)^{-1}$.

https://dx.doi.org/10.1021/acs.jpclett.1c00077
J. Phys. Chem. Lett. 2021, 12, 2213−2218

NsTA spectroscopy further certifies that $D^{\bullet+}$-$A^{\bullet-}$-$R^{\bullet} \rightarrow {}^3$*D-A-$R^{\bullet}$ as evidenced by a broad feature centered around 650 nm assigned to ^{3}*D (Figure 3b and Figure S4).[43] Because the observed rate constant is $k_{CR1}^{T} + k_{CR2}^{T}$, we cannot determine k_{CR1}^{T} independently using the data at 105 K. However, because the free energy change for $D^{\bullet+}$-^{3}($A^{\bullet-}$-$R^{\bullet}$) $\rightarrow$ D-A-$R^{\bullet}$ is about −2.25 eV, placing it well into the Marcus inverted region, we can assume that $k_{CR2}^{T} > k_{CR1}^{T}$ so that $k_{CR1}^{T} + k_{CR2}^{T} \simeq k_{CR2}^{T}$ because the more rapid CR reaction producing $D^{\bullet+}$-^{3}($A^{\bullet-}$-$R^{\bullet}$) $\rightarrow {}^3$*D-A-$R^{\bullet}$ occurs with $\Delta G_{CR2}^{T} \simeq -0.3$ eV and is close to the maximum of the Marcus rate vs free energy profile for $\lambda = 0.4$ eV. The fsTA and nsTA data for reference compound $D^{\bullet+}$-$A^{\bullet-}$-RH, **1H** in PrCN at 105 K show that the initial CS for **1H** occurs with a rate constant $k_{CS1} = (48.9 \pm 0.2\ \text{ps})^{-1}$, which is comparable to that of **1**, while the CR reaction for **1H** displays distributed kinetics with major components of $k_{CR1} = (38.7 \pm 0.5\ \text{ns})^{-1}$ and $k_{CR1'} = (228 \pm 4\ \text{ns})^{-1}$. These slow CR rates are consistent with the Marcus inverted region arguments given above.

To estimate the dielectric constant of PrCN at 105 K, we measured the rate constants for **1** and **1H** in toluene at 295 K for which $\varepsilon_s = 2.4$ (see Figures S8−S11). The rate constants obtained in toluene are all somewhat faster than those measured in PrCN at 105 K, which electron transfer theory[34,35] predicts is due to an increase in the radical ion pair energy that in turn implies that $\varepsilon_s < 2.4$ for PrCN at 105 K. The energy levels in Figure 1b are calculated by using $\varepsilon_s = 2.3$ as an example.

We observed an intense spin-polarized TREPR spectrum in PrCN at 105 K following selective photoexcitation of D in **1** at the X-band (~9.6 GHz). As described above, nsTA spectroscopy at 105 K shows that the only remaining species on the time scale of the TREPR experiment (>50 ns) is ^{3}*D-A-$R^{\bullet}$. Its TREPR spectrum displays an *e*, *a* (*a* = enhanced absorption, *e* = enhanced emission, low to high field) polarization pattern with a 0.8 mT splitting (peak-to-peak) and a 3.2 mT width (baseline-to-baseline) (Figure 4). If the magnetic field range is expanded to 260−420 mT, no additional lines are obvious above the noise (Figure S12). In addition, the TREPR spectrum of ^{3}*D was recorded under the same conditions as that of ^{3}*D-A-$R^{\bullet}$ to obtain the zero-field splitting parameters of ^{3}*D needed to fit the spectrum of ^{3}*D-A-$R^{\bullet}$. The Hamiltonian for a coupled triplet−doublet pair given in eq 1 was used to fit the spectrum of ^{3}*D-A-$R^{\bullet}$:[46]

$$\mathcal{H} = \omega_R \hat{S}_{R,z} + \omega_T \hat{S}_{T,z} + J_{TR}\boldsymbol{S}_R\boldsymbol{S}_T + \boldsymbol{S}_T\boldsymbol{D}_{TR}\boldsymbol{S}_R + \boldsymbol{S}_T\boldsymbol{D}_T\boldsymbol{S}_T \quad (1)$$

where ω_R and ω_T are the Larmor frequencies of the doublet ($R^{\bullet}$) and the triplet (^{3}*D), respectively; J_{TR} is the isotropic exchange coupling between the doublet and the triplet; $\boldsymbol{D}_{TR}$ is the doublet−triplet dipolar interaction tensor in the point-dipole approximation; $\boldsymbol{D}_T$ is the triplet zero-field splitting tensor; and $\hat{S}_{R,z}$, $\boldsymbol{S}_R$, $\hat{S}_{R,z}$, $\boldsymbol{S}_T$ are the spin operators of the doublet and the triplet spins. $\boldsymbol{D}_T$ was determined from the EPR spectrum of reference compound ^{3}*D, which yields $|D|$= 1824 MHz and $|E|$ = 360 MHz (Figure S13 and Table S3), and was fixed during the fitting process for ^{3}*D-A-$R^{\bullet}$. The fit parameters for the TREPR spectrum of ^{3}*D-A-$R^{\bullet}$ are given in Table S4.

The fit indicates that the TREPR spectrum of ^{3}*D-A-$R^{\bullet}$ is dominated by transitions of $R^{\bullet}$ because of the comparable magnitudes of relatively weak dipolar and exchange coupling between ^{3}*D and $R^{\bullet}$, such that the transitions of ^{3}*D at much higher and lower fields are very weak and do not appear above the noise level in the spectrum (see Figure S12). The *e*, *a* polarization pattern arises from the selective population of all four $m_s = \pm 1/2$ sublevels. This preferential population originates in spin-polarized ^{3}*D generated by the reaction $D^{\bullet+}$-^{3}($A^{\bullet-}$-$R^{\bullet}$) $\rightarrow {}^3$*D-A-$R^{\bullet}$ through the radical-pair intersystem crossing mechanism,[47−51] in which S−T_{+1} mixing occurs because the exchange interaction within the $D^{\bullet+}$-$A^{\bullet-}$ radical pair is comparable to the Zeeman splitting at the X-band (Figure 5).[52−54] Consequently, the spin polarization of ^{3}*D is transferred to $R^{\bullet}$ to the four $m_s = \pm 1/2$ states in the doublet−quartet manifold.[55−57] Because of the relatively small population difference between $m_s = \pm 1/2$ sublevels ($D_{+1/2}$ and $D_{-1/2}$, $Q_{+1/2}$ and $Q_{-1/2}$), the population differences between $Q_{-3/2}$ and $Q_{-1/2}$ and between $Q_{+1/2}$ and $Q_{+3/2}$ dominate; therefore, an overall *e*, *a* EPR spectrum is observed.

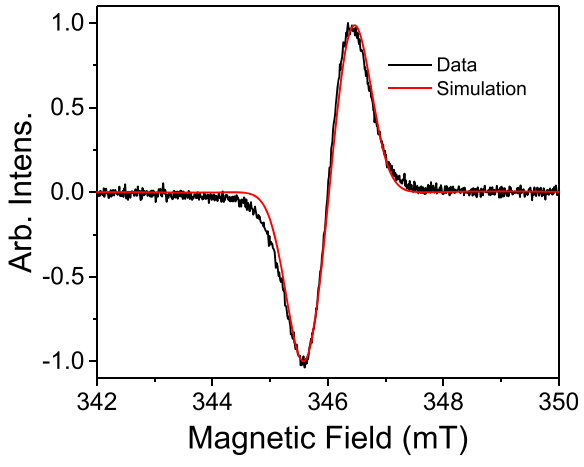

Figure 4. TREPR spectrum of **1** at the X-band in PrCN glass at 105 K, 100 ns after a 7 ns, 450 nm laser pulse. The simulation is shown in red.

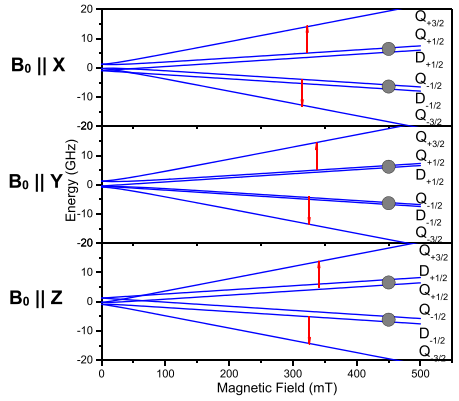

Figure 5. Schematic for EPR transitions in all three canonical orientations of the system relative to the magnetic field, B_0, with $m_s = \pm 1/2$ sublevels overpopulated. Gray circles represent the population differences of spin sublevels relative to the least populated sublevel, downward arrows represent emissive transitions, and upward arrows represent absorptive transitions.

These results show that tuning the energetics of a D-A-$R^{\bullet}$ molecule by changing its dielectric environment can achieve the charge transfer reaction mechanisms necessary to strongly

https://dx.doi.org/10.1021/acs.jpclett.1c00077
J. Phys. Chem. Lett. 2021, 12, 2213−2218

polarize an adjacent radical to serve as a spin qubit with a well-defined spin state or to generate the intermediates necessary to carry out quantum teleportation experiments using the same molecule, thus providing a flexible three-qubit system for future quantum logic gate and spin-state teleportation experiments.

■ ASSOCIATED CONTENT

Supporting Information

The Supporting Information is available free of charge at https://pubs.acs.org/doi/10.1021/acs.jpclett.1c00077.

Experimental details, including synthesis, NMR, mass spectrometry, steady-state absorption, electrochemistry, additional TA spectra and kinetics, TREPR spectra and simulation parameters. (PDF)

■ AUTHOR INFORMATION

Corresponding Author

Michael R. Wasielewski − *Department of Chemistry, Center for Molecular Quantum Transduction, and Institute for Sustainability and Energy at Northwestern, Northwestern University, Evanston, Illinois 60208-3113, United States;* orcid.org/0000-0003-2920-5440; Email: m-wasielewski@northwestern.edu

Authors

Haochuan Mao − *Department of Chemistry, Center for Molecular Quantum Transduction, and Institute for Sustainability and Energy at Northwestern, Northwestern University, Evanston, Illinois 60208-3113, United States;* orcid.org/0000-0001-8742-089X

Ryan M. Young − *Department of Chemistry, Center for Molecular Quantum Transduction, and Institute for Sustainability and Energy at Northwestern, Northwestern University, Evanston, Illinois 60208-3113, United States;* orcid.org/0000-0002-5108-0261

Matthew D. Krzyaniak − *Department of Chemistry, Center for Molecular Quantum Transduction, and Institute for Sustainability and Energy at Northwestern, Northwestern University, Evanston, Illinois 60208-3113, United States;* orcid.org/0000-0002-8761-7323

Complete contact information is available at: https://pubs.acs.org/10.1021/acs.jpclett.1c00077

Notes

The authors declare no competing financial interest.

■ ACKNOWLEDGMENTS

The authors thank Drs. Brandon Rugg and Jinyuan Zhang for providing synthetic intermediates and helpful discussions. This work was supported by the National Science Foundation under Award CHE-1900422.

■ REFERENCES

(1) Harrow, A. W.; Montanaro, A. Quantum computational supremacy. *Nature* **2017**, *549*, 203−209.

(2) Degen, C. L.; Reinhard, F.; Cappellaro, P. Quantum sensing. *Rev. Mod. Phys.* **2017**, *89*, 035002.

(3) Biamonte, J.; Wittek, P.; Pancotti, N.; Rebentrost, P.; Wiebe, N.; Lloyd, S. Quantum machine learning. *Nature* **2017**, *549*, 195−202.

(4) Wasielewski, M. R.; Forbes, M. D. E.; Frank, N. L.; Kowalski, K.; Scholes, G. D.; Yuen-Zhou, J.; Baldo, M. A.; Freedman, D. E.; Goldsmith, R. H.; Goodson, T., III; et al. Exploiting chemistry and molecular systems for quantum information science. *Nat. Rev. Chem.* **2020**, *4*, 490−504.

(5) Atzori, M.; Sessoli, R. The second quantum revolution: Role and challenges of molecular chemistry. *J. Am. Chem. Soc.* **2019**, *141*, 11339−11352.

(6) Troiani, F.; Affronte, M. Molecular spins for quantum information technologies. *Chem. Soc. Rev.* **2011**, *40*, 3119−3129.

(7) Liu, Y.; Toma, F. M. Catalyst: Qubits from the bottom up. *Chem.* **2020**, *6*, 795−798.

(8) Takui, T.; Berliner, L.; Hanson, G. *Electron Spin Resonance (ESR) Based Quantum Computing*; Springer: 2016; Vol. *31*.

(9) Sato, K.; Nakazawa, S.; Rahimi, R.; Ise, T.; Nishida, S.; Yoshino, T.; Mori, N.; Toyota, K.; Shiomi, D.; Yakiyama, Y.; et al. Molecular electron-spin quantum computers and quantum information processing: Pulse-based electron magnetic resonance spin technology applied to matter spin-qubits. *J. Mater. Chem.* **2009**, *19*, 3739−3754.

(10) Coronado, E. Molecular magnetism: From chemical design to spin control in molecules, materials and devices. *Nat. Rev. Mater.* **2020**, *5*, 87−104.

(11) Zadrozny, J. M.; Niklas, J.; Poluektov, O. G.; Freedman, D. E. Millisecond coherence time in a tunable molecular electronic spin qubit. *ACS Cent. Sci.* **2015**, *1*, 488−492.

(12) Lombardi, F.; Lodi, A.; Ma, J.; Liu, J.; Slota, M.; Narita, A.; Myers, W. K.; Müllen, K.; Feng, X.; Bogani, L. Quantum units from the topological engineering of molecular graphenoids. *Science* **2019**, *366*, 1107−1110.

(13) Shiddiq, M.; Komijani, D.; Duan, Y.; Gaita-Ariño, A.; Coronado, E.; Hill, S. Enhancing coherence in molecular spin qubits via atomic clock transitions. *Nature* **2016**, *531*, 348−351.

(14) Yu, C. J.; Krzyaniak, M. D.; Fataftah, M. S.; Wasielewski, M. R.; Freedman, D. E. A concentrated array of copper porphyrin candidate qubits. *Chem. Sci.* **2019**, *10*, 1702−1708.

(15) Gaita-Ariño, A.; Luis, F.; Hill, S.; Coronado, E. Molecular spins for quantum computation. *Nat. Chem.* **2019**, *11*, 301−309.

(16) Zadrozny, J. M.; Gallagher, A. T.; Harris, T. D.; Freedman, D. E. A porous array of clock qubits. *J. Am. Chem. Soc.* **2017**, *139*, 7089−7094.

(17) Fernandez, A.; Ferrando-Soria, J.; Pineda, E. M.; Tuna, F.; Vitorica-Yrezabal, I. J.; Knappke, C.; Ujma, J.; Muryn, C. A.; Timco, G. A.; Barran, P. E.; Ardavan, A.; Winpenny, R. E. P. Making hybrid [n]-rotaxanes as supramolecular arrays of molecular electron spin qubits. *Nat. Commun.* **2016**, *7*, 10240.

(18) Nakazawa, S.; Nishida, S.; Ise, T.; Yoshino, T.; Mori, N.; Rahimi, R. D.; Sato, K.; Morita, Y.; Toyota, K.; Shiomi, D.; et al. A synthetic two-spin quantum bit: G-engineered exchange-coupled biradical designed for controlled-not gate operations. *Angew. Chem., Int. Ed.* **2012**, *51*, 9860−9864.

(19) Rugg, B. K.; Krzyaniak, M. D.; Phelan, B. T.; Ratner, M. A.; Young, R. M.; Wasielewski, M. R. Photodriven quantum teleportation of an electron spin state in a covalent donor-acceptor-radical system. *Nat. Chem.* **2019**, *11*, 981−986.

(20) Nelson, J. N.; Zhang, J.; Zhou, J.; Rugg, B. K.; Krzyaniak, M. D.; Wasielewski, M. R. CNOT gate operation on a photogenerated molecular electron spin-qubit pair. *J. Chem. Phys.* **2020**, *152*, 014503.

(21) Olshansky, J. H.; Zhang, J.; Krzyaniak, M. D.; Lorenzo, E. R.; Wasielewski, M. R. Selectively addressable photogenerated spin qubit pairs in DNA hairpins. *J. Am. Chem. Soc.* **2020**, *142*, 3346−3350.

(22) Aguila, D.; Barrios, L. A.; Velasco, V.; Roubeau, O.; Repolles, A.; Alonso, P. J.; Sese, J.; Teat, S. J.; Luis, F.; Aromi, G. Heterodimetallic [LnLn'] lanthanide complexes: Toward a chemical design of two-qubit molecular spin quantum gates. *J. Am. Chem. Soc.* **2014**, *136*, 14215−14222.

(23) Fernandez, A.; Moreno Pineda, E.; Muryn, C. A.; Sproules, S.; Moro, F.; Timco, G. A.; McInnes, E. J. L.; Winpenny, R. E. P. *g*-engineering in hybrid rotaxanes to create AB and AB_2 electron spin systems: EPR spectroscopic studies of weak interactions between dissimilar electron spin qubits. *Angew. Chem., Int. Ed.* **2015**, *54*, 10858−10861.

(24) Atzori, M.; Chiesa, A.; Morra, E.; Chiesa, M.; Sorace, L.; Carretta, S.; Sessoli, R. A two-qubit molecular architecture for electron-mediated nuclear quantum simulation. *Chem. Sci.* **2018**, *9*, 6183−6192.
(25) Bayliss, S. L.; Laorenza, D. W.; Mintun, P. J.; Kovos, B. D.; Freedman, D. E.; Awschalom, D. D. Optically addressable molecular spins for quantum information processing. *Science* **2020**, *370*, 1309−1312.
(26) Warren, W. S. The usefulness of NMR quantum computing. *Science* **1997**, *277*, 1688−1690.
(27) Thurnauer, M. C.; Norris, J. R. An electron spin echo phase shift observed in photosynthetic algae: Possible evidence for dynamic radical pair interactions. *Chem. Phys. Lett.* **1980**, *76*, 557−561.
(28) Buckley, C. D.; Hunter, D. A.; Hore, P. J.; McLauchlan, K. A. Electron spin resonance of spin-correlated radical pairs. *Chem. Phys. Lett.* **1987**, *135*, 307−312.
(29) Chen, H. F.; Gardner, D. M.; Carmieli, R.; Wasielewski, M. R. Controlling the orientation of spin-correlated radical pairs by covalent linkage to nanoporous anodic aluminum oxide membranes. *Chem. Commun.* **2013**, *49*, 8614−6.
(30) Horwitz, N. E.; Phelan, B. T.; Nelson, J. N.; Mauck, C. M.; Krzyaniak, M. D.; Wasielewski, M. R. Spin polarization transfer from a photogenerated radical ion pair to a stable radical controlled by charge recombination. *J. Phys. Chem. A* **2017**, *121*, 4455−4463.
(31) Horwitz, N. E.; Phelan, B. T.; Nelson, J. N.; Krzyaniak, M. D.; Wasielewski, M. R. Picosecond control of photogenerated radical pair lifetimes using a stable third radical. *J. Phys. Chem. A* **2016**, *120*, 2841−2853.
(32) Colvin, M. T.; Carmieli, R.; Miura, T.; Richert, S.; Gardner, D. M.; Smeigh, A. L.; Dyar, S. M.; Conron, S. M.; Ratner, M. A.; Wasielewski, M. R. Electron spin polarization transfer from photogenerated spin-correlated radical pairs to a stable radical observer spin. *J. Phys. Chem. A* **2013**, *117*, 5314−5325.
(33) Mi, Q.; Chernick, E. T.; McCamant, D. W.; Weiss, E. A.; Ratner, M. A.; Wasielewski, M. R. Spin dynamics of photogenerated triradicals in fixed distance electron donor-chromophore-acceptor-tempo molecules. *J. Phys. Chem. A* **2006**, *110*, 7323−7333.
(34) Marcus, R. A. On the theory of oxidation-reduction reactions involving electron transfer. I. *J. Chem. Phys.* **1956**, *24*, 966−978.
(35) Marcus, R. A. On the theory of electron-transfer reactions. VI. Unified treatment for homogeneous and electrode reactions. *J. Chem. Phys.* **1965**, *43*, 679−701.
(36) Weller, A. Photoinduced electron transfer in solution: Exciplex and radical ion pair formation free enthalpies and their solvent dependence. *Z. Phys. Chem.* **1982**, *133*, 93−98.
(37) Salikhov, K. M.; Golbeck, J. H.; Stehlik, D. Quantum teleportation across a biological membrane by means of correlated spin pair dynamics in photosynthetic reaction centers. *Appl. Magn. Reson.* **2007**, *31*, 237−252.
(38) van der Est, A.; Asano-Someda, M.; Ragogna, P.; Kaizu, Y. Light-induced electron spin polarization of a weakly coupled triplet-doublet spin pair in a covalently linked porphyrin dimer. *J. Phys. Chem. A* **2002**, *106*, 8531−8542.
(39) Kandrashkin, Y. E.; van der Est, A. The triplet mechanism of electron spin polarization in moderately coupled triplet-doublet rigid complexes as a source of the enhanced + 1/2/−1/2 transitions. *J. Chem. Phys.* **2019**, *151*, 184301.
(40) Young, R. M.; Dyar, S. M.; Barnes, J. C.; Juricek, M.; Stoddart, J. F.; Co, D. T.; Wasielewski, M. R. Ultrafast conformational dynamics of electron transfer in $ExBox^{4+}$ > perylene. *J. Phys. Chem. A* **2013**, *117*, 12438−12448.
(41) Gosztola, D.; Niemczyk, M. P.; Svec, W.; Lukas, A. S.; Wasielewski, M. R. Excited doublet states of electrochemically generated aromatic imide and diimide radical anions. *J. Phys. Chem. A* **2000**, *104*, 6545−6551.
(42) Christensen, J. A.; Zhang, J.; Zhou, J.; Nelson, J. N.; Wasielewski, M. R. Near-infrared excitation of the peri-xanthenoxanthene radical cation drives energy-demanding hole transfer reactions. *J. Phys. Chem. C* **2018**, *122*, 23364−23370.
(43) Al-Aqar, R.; Benniston, A. C.; Harriman, A.; Perks, T. Structural dynamics and barrier crossing observed for a fluorescent O-doped polycyclic aromatic hydrocarbon. *ChemPhotoChem.* **2017**, *1*, 198−205.
(44) Rugg, B. K.; Phelan, B. T.; Horwitz, N. E.; Young, R. M.; Krzyaniak, M. D.; Ratner, M. A.; Wasielewski, M. R. Spin-selective photoreduction of a stable radical within a covalent donor-acceptor-radical triad. *J. Am. Chem. Soc.* **2017**, *139*, 15660−15663.
(45) Phelan, B. T.; Zhang, J.; Huang, G.-J.; Wu, Y.-L.; Zarea, M.; Young, R. M.; Wasielewski, M. R. Quantum coherence enhances electron transfer rates to two equivalent electron acceptors. *J. Am. Chem. Soc.* **2019**, *141*, 12236−12239.
(46) Stoll, S.; Schweiger, A. Easyspin, a comprehensive software package for spectral simulation and analysis in EPR. *J. Magn. Reson.* **2006**, *178*, 42−55.
(47) Colvin, M. T.; Ricks, A. B.; Scott, A. M.; Smeigh, A. L.; Carmieli, R.; Miura, T.; Wasielewski, M. R. Magnetic field-induced switching of the radical-pair intersystem crossing mechanism in a donor-bridge-acceptor molecule for artificial photosynthesis. *J. Am. Chem. Soc.* **2011**, *133*, 1240−3.
(48) Miura, T.; Carmieli, R.; Wasielewski, M. R. Time-resolved EPR studies of charge recombination and triplet-state formation within donor-bridge-acceptor molecules having wire-like oligofluorene bridges. *J. Phys. Chem. A* **2010**, *114*, 5769−5778.
(49) Colvin, M. T.; Ricks, A. B.; Scott, A. M.; Co, D. T.; Wasielewski, M. R. Intersystem crossing involving strongly spin exchange-coupled radical ion pairs in donor-bridge-acceptor molecules. *J. Phys. Chem. A* **2012**, *116*, 1923−1930.
(50) van Willigen, H.; Jones, G.; Farahat, M. S. Time-resolved EPR study of photoexcited triplet-state formation in electron-donor-substituted acridinium ions. *J. Phys. Chem.* **1996**, *100*, 3312−3316.
(51) Levanon, H.; Norris, J. R. The photoexcited triplet state and photosynthesis. *Chem. Rev.* **1978**, *78*, 185−198.
(52) Adrian, F.; Monchick, L. Theory of chemically induced magnetic polarization. Effects of S-$T_{\pm1}$ mixing in strong magnetic fields. *J. Chem. Phys.* **1979**, *71*, 2600−2610.
(53) Adrian, F.; Monchick, L. Analytic formula for chemically induced magnetic polarization by S-$T_{\pm1}$ mixing in a strong magnetic field. *J. Chem. Phys.* **1980**, *72*, 5786−5787.
(54) Honma, H.; Murai, H.; Kuwata, K. CIDEP study on photooxidation of *N, N, N′, N′*-tetramethyl-*p*-phenylenediamine by maleic anhydride. Enhanced S-T_{-1} mixing by radical-ion pair system. *Chem. Phys. Lett.* **1992**, *195*, 239−242.
(55) Kandrashkin, Y. E.; van der Est, A. Stimulated electron spin polarization in strongly coupled triplet-doublet spin pairs. *Appl. Magn. Reson.* **2011**, *40*, 189−204.
(56) Avalos, C. E.; Richert, S.; Socie, E.; Karthikeyan, G.; Casano, G.; Stevanato, G.; Kubicki, D. J.; Moser, J. E.; Timmel, C. R.; Lelli, M.; et al. Enhanced intersystem crossing and transient electron spin polarization in a photoexcited pentacene-trityl radical. *J. Phys. Chem. A* **2020**, *124*, 6068−6075.
(57) Nolden, O.; Fleck, N.; Lorenzo, E. R.; Wasielewski, M. R.; Schiemann, O.; Gilch, P.; Richert, S. Excitation energy transfer and exchange-mediated quartet state formation in porphyrin-trityl systems. *Chem. - Eur. J.* **2021**, *27*, 2683−2691.

https://dx.doi.org/10.1021/acs.jpclett.1c00077
J. Phys. Chem. Lett. 2021, 12, 2213−2218